Food Research International 105 (2018) 129–139

Contents lists available at ScienceDirect

Food Research International

journal homepage: www.elsevier.com/locate/foodres

Relationship between nano/micro structure and physical properties of TiO_2-sodium caseinate composite films☆

Juan Manuel Montes-de-Oca-Ávalos[a,1], Davide Altamura[b,1], Roberto Jorge Candal[c], Francesco Scattarella[b], Dritan Siliqi[b], Cinzia Giannini[b,*], María Lidia Herrera[a,*]

[a] Institute of Polymer Technology and Nanotechnology, University of Buenos Aires-CONICET, Faculty of Engineering, Las Heras 2214, C1127AAQ Ciudad de Buenos Aires, Argentina
[b] Institute of Crystallography, National Research Council, 122/O Amendola, I-70126 Bari, Italy
[c] Instituto de Investigación e Ingeniería Ambiental, Universidad Nacional de San Martín - CONICET, Campus Miguelete, 25 de Mayo y Francia, 1650 San Martín, Provincia de Buenos Aires, Argentina

ARTICLE INFO

Keywords:
Sodium caseinate films
TiO_2 nanoparticles
Gel
Conventional emulsion
Nanoemulsions
SAXS/WAXS
Mechanical properties
Water vapor permeability

ABSTRACT

Films obtained by casting, starting from conventional emulsions (CE), nanoemulsions (NE) or their gels, which led to different structures, with the aim of explore the relationship between structure and physical properties, were prepared. Sodium caseinate was used as the matrix, glycerol as plasticizer, glucono-delta-lactone as acidulant to form the gels, and TiO_2 nanoparticles as reinforcement to improve physical behavior. Structural characterization was performed by SAXS and WAXS (Small and Wide Angle X-ray Scattering, respectively), combined with confocal and scanning electron microscopy. The results demonstrate that the incorporation of the lipid phase does not notably modify the mechanical properties of the films compared to solution films. Films from NE were more stable against oil release than those from CE. Incorporation of TiO_2 improved mechanical properties as measured by dynamical mechanical analysis (DMA) and uniaxial tensile tests. TiO_2 macroscopic spatial distribution homogeneity and the nanostructure character of NE films were confirmed by mapping the q-dependent scattering intensity in scanning SAXS experiments. SAXS microscopies indicated a higher intrinsic homogeneity of NE films compared to CE films, independently of the TiO_2 load. NE-films containing structures with smaller and more homogeneously distributed building blocks showed greater potential for food applications than the films prepared from sodium caseinate solutions, which are the best known films.

1. Introduction

Packaging is determinant for storage and preservation of food. For perishable food, sometimes a gas and water vapor barrier is necessary to preserve the quality of the products throughout their lifecycle. These characteristics are typically achieved by using multilayer film barrier. Multilayer packaging materials used at present are mostly no recyclable, neither biodegradable (Cinelli et al., 2014). Following the new tendency of reducing environmental impact, it is necessary to develop films with high barrier properties based on biodegradable and renewable materials. Biopolymers from proteins and carbohydrates were tested with those purposes, showing promising mechanical and physicochemical properties. However, it is still necessary to improve their physical behavior (Wihodo & Moraru, 2013). Additionally, food packaging was not only designed to protect the contents, but also thought to incorporate different ingredients to bring special benefits. Such is the case of the incorporation of environmental friendly bactericides or vitamins precursors (Arrieta et al., 2014; Arrieta, Peltzer, Garrigós, & Jiménez, 2013; Moditsi, Lazaridou, Moschakis, & Biliaderis, 2014; Valencia-Chamorro, Palou, del Río, & Pérez-Gago, 2011).

Several articles in literature deal with addition of hydrophobic substances into the biopolymer film, such as vegetable oils (Pereda, Aranguren, & Marcovich, 2010), essential oils (Acevedo-Fani, Salvia-Trujillo, Rojas-Grau, & Martín-Belloso, 2015; Atarés, Bonilla, & Chiralt, 2010; Zinoviadou, Koutsoumanis, & Biliaderis, 2009), fatty acids (Reznavi, Schleining, Sümen, & Taherian, 2013), waxes (Perez-Gago & Krochta, 2001), fatty acids and waxes (Fabra, Talens, Gavara, & Chiralt, 2012), or naturally emulsified oil bodies (Matsakidou, Biliaderis, &

☆ Conflicts of interest: None.

* Corresponding authors.
E-mail addresses: davide.altamura@ic.cnr.it (D. Altamura), francesco.scattarella@ic.cnr.it (F. Scattarella), dritan.siliqi@ic.cnr.it (D. Siliqi), cinzia.giannini@ic.cnr.it (C. Giannini), mlidiaherrera@gmail.com (M.L. Herrera).

[1] These authors (J. M. M. de O. A. and D. A.) contributed equally.

https://doi.org/10.1016/j.foodres.2017.11.011
Received 27 September 2017; Received in revised form 30 October 2017; Accepted 13 November 2017
Available online 14 November 2017
0963-9969/

Kiosseoglou, 2013). The substances were included in the matrix to improve water vapor permeability (WVP) properties. Most of those films were formed from solutions or emulsions with droplet sizes in the conventional range (> 100 nm). Although nanoemulsions may improve performance of films due to their higher stability and droplet size homogeneity, the behavior of the resulting films is not very well known yet. The advantage of using oil-in-water (O/W) emulsions stabilized by proteins (for example caseinate or whey protein), in the presence of a plasticizer, is that the films may contain functional ingredients dissolved in the oil micelles (Helal, Tagliazucchi, Conte, & Desobry, 2012; Jiménez, Fabra, Talens, & Chiralt, 2013; Pereda et al., 2010). These substances may be slowly released to the package content, or remain inside preventing microbiological infection (Navarro, Arancibia, Herrera, & Matiacevich, 2016; Colak, Gouanve, Degraeve, Espuche, & Prochazka, 2015; Bonilla & Sobral, 2017).

It was reported that TiO_2 nanoparticles homogeneously dispersed in films prepared from whey protein isolated (Li et al., 2011; Zhou, Wang, & Gunasekaran, 2009), soy protein isolate (Wang et al., 2013), or films prepared from a mixed solution of whey protein isolate and sodium caseinate (Lei et al., 2014) acted as mechanical reinforcement and gas barrier against gas or vapor permeability in the right concentrations. Due to its low toxicity and chemical inertness, TiO_2 was appropriate for applications in food packaging. Besides, nano-TiO_2 incorporated into protein films displayed antimicrobial activity against both *E. coli* and *S. aureus* (Lei et al., 2014). Thus, it is interesting to study its effect in films prepared from emulsions or gels since the microstructure, mechanical and barrier properties of the films may depend on nanoparticles organization, distribution and interaction with the polymeric matrix (Frohberg, Pietzsch, & Ulrich, 2010).

Establishing the correlation between microstructure and physical properties is very important for the design of novel films. The characterization of these advanced materials includes the application of powerful X-ray techniques that provide structural information. In this sense, X-ray scattering techniques such as SAXS and WAXS (Small and Wide Angle X-ray Scattering, respectively) are suitable for the structural characterization of materials containing dispersed crystalline phases. SAXS mainly provides morphological information on the structural arrangement at the nanoscale of the non-crystalline phase (the matrix) as well as of crystalline nanoparticles. WAXS provides structural information on the crystalline phase. There are only a few reports using these techniques to describe biodegradable materials but none of them described sodium caseinate films (Hwang, Yoo, & Im, 2011; Morales, Franco, Casas, & Puiggali, 2010; Tsai et al., 2010; Wang et al., 2013). In this study, the combination of both techniques allowed a deep description on the microstructure of the polymer films, including the spatial distribution of the submicrometric charge, the TiO_2 nanoparticles.

The aim of the present work is to explore the preparation of new biodegradable edible films based on sodium caseinate and reinforced by nanoparticles of TiO_2 starting from different systems: gel, conventional emulsions or nanoemulsions. Structural and physical characterization of all systems was performed to interpret their mechanical behavior.

2. Materials and methods

2.1. Starting materials

Sodium caseinate (NaCas) was obtained from ICN (ICN Biomedical, Inc., Aurora, Ohio, USA). Glucono-δ-lactone (GDL) was purchased from Sigma-Aldrich, Co. (St. Louis, MO, USA). Glycerol was of analytical grade from Chemit (Chemit, Buenos Aires, Argentina). Sunflower oil (SFO) was of commercial origin. Its main fatty acids were palmitic, stearic, oleic and linoleic acids with percentages of 6.1%, 3.0%, 23.1%, and 67.3%, respectively. Deionized water (18 mΩ; Milli-Q Water System, Millipore Corporation, Billerica, MA, USA) was used for all experiments. Degussa P 25 (TiO2) from Evonik (Evonik, Essen, Germany) was used as charge.

2.2. Films preparation

Films were prepared from conventional emulsions (CE), nanoemulsions (NE), or their gels i.e. gel prepared from conventional emulsions (CG), and gel prepared from nanoemulsions (NG). Films were also prepared from solutions (S) in order to compare our results with the ones published in literature. All samples, contained 2.5 wt% NaCas, and 2 wt% glycerol. CE, NE, CG, and NG also contained 1 wt% SFO. Films may or may not contain TiO_2. TiO_2 was added as a charge in concentrations of 0.5 wt%. These films were named: CET0.5, NET0.5, CGT0.5 or NGT0.5, when were prepared from CE, NE, CG or NG respectively. The optimum concentration was selected taking into account mechanical and tensile properties evaluated in CE in a range that varied from 0.1 to 1 wt%. Glycerol concentration was also selected taking into account mechanical properties of films prepared from CE (data shown in Section 3.1).

To prepare CE, oil and aqueous phases were mixed using an Ultra-Turrax (UT) T8 high speed blender (S 8N-5G dispersing tool, IKA Labortechnik, Janke & Kunkel, GmbH & Co., Staufen, Germany), operated at 20,000 rpm for 1 min. Samples were kept in an ice bath (0 °C) during processing. Coarse emulsions were obtained after repeating this process three times. The resultant coarse emulsions were further homogenized for 20 min using an ultrasonic liquid processing (US), VIBRA CELL, VC750 (power 750 W, frequency 20 kHz) model (Sonics & Materials, Inc., Newtown, CT, USA), with a 13-mm-diameter and 136-mm-length tip and an amplitude of 30%. The temperature of the sample-cell was controlled by means of an ice bath (0 °C) with a temperature cut down control of 20 ± 1 °C during ultrasound treatment. Average droplet sizes of the distribution expressed in volume varied from 0.2 to 0.6 μm.

NE were prepared using a combination of a high-energy homogenization and evaporative ripening methods previously reported for whey protein-stabilized systems with some minor changes (Lee & McClements, 2010). In nanoemulsions, oil phase was a blend of SFO and ethyl acetate. The conventional emulsions obtained after ultrasound treatment were placed in a rotary evaporator Buchi model R 100 (Buchi, Postfach, Switzerland) connected to a vacuum pump and a recirculating chiller to eliminate ethyl acetate. The degree of ethyl acetate evaporation was determined by carrying out a mass balance of emulsions before and after solvent evaporation. The process was performed at 45 °C for 20 min. After evaporation, enough amount of water was added to the samples in order to keep constant the composition of aqueous phase. Then, the samples were cooled quiescently to 25 °C. The average diameter of droplets (Z-average) varied from 40 to 60 nm.

For gel formation, selected acidulant was GDL which was used at a concentration of 1 wt%. The final pH value was 4.75 ± 0.20. The required amount of GDL was accurately weighted and added to 10 g of CE or NE. GDL was dissolved by stirring tubes with a vortex.

Films were prepared by casting, placing 8 g of conventional emulsion, or nanoemulsion, with or without addition of GDL or TiO_2, in a disposable polystyrene weighing dish with a 6 cm of diameter. Films from NaCas solution were also prepared. In the case of films from gels, the gels were formed at ambient temperature by keeping samples in the dish for 2 h before drying. Then, the dishes were placed in an oven set at 40 °C for 24 h. After preparation, films were stored in desiccators exposed to an atmosphere of saturated solution of $Ca(NO_3)_2$, (water activity 0.53).

2.3. Films characterization

2.3.1. Mechanical and tensile properties

Complex (E*), storage (E′) and loss (E″) moduli were measured by dynamic mechanical analysis (DMA) using a DMA 8000 Perkin Elmer (Perkin Elmer, Chicago, USA) with controlled temperature and

humidity chamber. Experiments were performed in tension mode and within the linear viscoelastic range applying a deformation of 0.05%. Temperature was kept at 25 °C and humidity at 53%. Values of moduli were obtained for a frequency scan from 1 to 10 Hz. Films were measured using clamps for tensile tests. The specimens were rectangular slabs (40 mm × 8 mm × 0.18 mm) and the dimensions were measured with an accuracy of 0.01 mm. Reported results are the average of three replicates.

Uniaxial tensile parameters values, Young modulus (E), the ultimate strength (σ_b), and elongation at break (ε_b), were obtained from stress-strain curves measured using an Instron dynamometer model 5982 (Instron, Norwood, USA). Tests were performed at a crosshead speed of 10 mm/min, and a temperature of 25.00 ± 0.01 °C, following standard test method for tensile properties of plastics by use of microtensile specimens (ASTM D1708). Eight specimens of samples cut out from the different matrix films were tested from a minimum of three films per sample. Results were reported as average and standard deviation.

2.3.2. Film barrier properties

Water vapor permeability (WVP) of the films was determined at room temperature using a modified ASTM E96-00 procedure (Famá, Rojo, Bernal, & Goyanes, 2012). Films were sealed on top of an acrylic permeation cell with an internal diameter of 50 mm and a depth of 35 mm containing $CaCl_2$. The cells were placed in desiccators with a constant relative humidity (RH) of 75%. Water vapor transport (WVT) was determined from the weight increase of the system from permeation, measuring over 24 h for 10 days. WVP was calculated as follow:

$$\mathrm{WVP} = \frac{\mathrm{WVT} \times e}{P_0 \times \mathrm{RH}} \quad (1)$$

where "e" is the film thickness and "P_0" is the saturation vapor pressure of water at room temperature. Test was made in triplicate and results were expressed as average and standard deviation.

2.3.3. Thermogravimetric properties

Thermogravimetric analysis (TGA) was performed using a Shimadzu TGA-50 analyzer (Shimadzu, Tokyo, Japan). Films were studied by heating a precisely weighted amount of sample (typically between 4.0 and 5.0 mg) in an inert nitrogen atmosphere from 25 to 500 °C at a heating rate of 10 °C/min. Nitrogen flow rate was 30 mL/min.

2.3.4. Microstructure by Laser Scanning Confocal Microscopy (LSCM)

The Olympus FV300 (Olympus Ltd., London, UK) CLSM with an Ar gas laser (λ = 488 nm) was used to collect the images. A 10 × ocular was used, together with a 60 × objective for a visual magnification of 600 ×. The laser intensity used was 10%. Images were recorded by using the confocal assistant software Olympus FluoView version 4.1 provided with the FV300 CLSM. Nile red was used to stain the lipid phase while Rhodamine B to analyze protein phase. Two sets of experiments were performed for each film, each of one contained only one dye. An amount of 0.5 mg of Nile red or 0.5 mg Rhodamine B was added to 5 mL of conventional emulsions or nanoemulsions formulated with or without 0.5 wt% TiO_2, and with or without 1 wt% GDL. Squares of 2 mm × 2 mm were cut and placed on microscope slides to obtain images.

2.3.5. Microstructure by Scanning Electron Microscopy (SEM)

Films of 1 mm × 1 mm were mounted on carbon tape placed on metal grids and examined with a Carl Zeiss SEM, FEG-SEM model Supra 40 (Zeiss, Oberkochen, Germany), operated at 3 kV, on the surface exposed to air during drying. The micrographs were taken at magnifications of 1000; 10,000; 50,000 or in some samples that gave well-defined images 100,000 × was also used. Conventional emulsions were not analyzed by this technique since they released oil and blurry images were obtained for these systems.

In addition to film surface, cryogenic fracture surfaces were observed. Films were frozen with liquid nitrogen and broken to expose cross-sectional area. In all cases, the top edge corresponded to the surface exposed to air during drying. Magnification was the same as for surface analysis.

2.3.6. X-ray characterization

SAXS and WAXS data were collected from films (in transmission mode) by a Rigaku Fr-E + Superbright Cu microsource, coupled to a three-pinhole camera through a focusing optics (Altamura et al., 2012). Two image plate detectors (IP) with 100 μm pixel size and off-line RAXIA reader were used to collect simultaneously SAXS and WAXS data from the same sample region (data not shown). The sample was kept at ambient pressure and temperature, being isolated from the vacuum flight tube by Kapton windows. In order to obtain better data quality, measurements were repeated on selected samples (i.e. CE and NE films, with and without TiO_2 charge, and NG films) kept in vacuum, by collecting SAXS data in scanning mode, with a 0.2 mm lateral step, by a Triton multiwire detector. The transmission maps were collected simultaneously by a small pin-diode detector in the beam stop. The comparison between SAXS data collected in these two configurations, allowed to conclude that the vacuum pressure (10^{-1} mbar) in the sample chamber did not significantly alter the sample structure, so that more accurate evaluations of the scattered intensity could be made, in particular concerning the presence of nanoscale objects. The scripts for the scanning experiments and the collected data were respectively written and processed by the SUNBIM software developed at CNR-IC (Siliqi et al., 2016) to obtain the SAXS and absorption contrast microscopies. SAXS curves were analyzed by using the program GNOM (Svergun, 1992) of the ATSAS suite (Franke et al., 2017), to calculate the Pair Distribution Function as the Fourier transform of the raw data, and adjusting the maximum object size (D_{max}) to obtain the best agreement of the back Fourier transform with the experimental SAXS profile. For each sample, ten SAXS profiles from consecutive points on the sample were added, in order to improve the signal to noise ratio.

2.4. Statistical analysis

For mechanical and tensile properties, water vapor permeability, and thermogravimetric analysis, significant differences between means were determined by the Student's *t*-test. An α level of 0.05 was used for significance. Results were reported as mean and standard deviation.

3. Results and discussion

3.1. Optimization of charge and glycerol concentrations

Fig. 1 shows mechanical and tensile properties for films prepared from CE. Films were formulated without charge or with addition of 0.1 to 1.0 wt% TiO_2. Part (a) reports the effect of TiO_2 on elastic modulus (E′), and part (b), (c), and (d), the effect on tensile parameters: Young modulus (E), the ultimate strength (σ_b), and elongation at break (ε_b), respectively. Addition of very low amounts of TiO_2 (lower than 0.3 wt %) diminished E' and did not improved parameters E, σ_b or ε_b. Low amounts of charge disrupted protein structure in some regions because TiO_2 modified protein molecules interactions. As a result of interference, films showed poorer mechanical properties. Addition of 0.5 wt %, however, significantly increased E', E, and σ_b, and decreased ε_b indicating that TiO_2 improved protein molecules organization added in this amount. This effect is likely consequence of the strong interaction between protein carboxylic groups and TiO_2 surface sites (Zhou et al., 2009). Higher amounts of charge led to worst properties than for films with 0.5 wt%. It was expected because for addition of 1 wt%, aggregates of TiO_2 with non-homogeneous distribution were evident at naked eye. Therefore 0.5 wt% TiO_2 was selected as charge concentration.

For glycerol concentration, the same analysis was performed

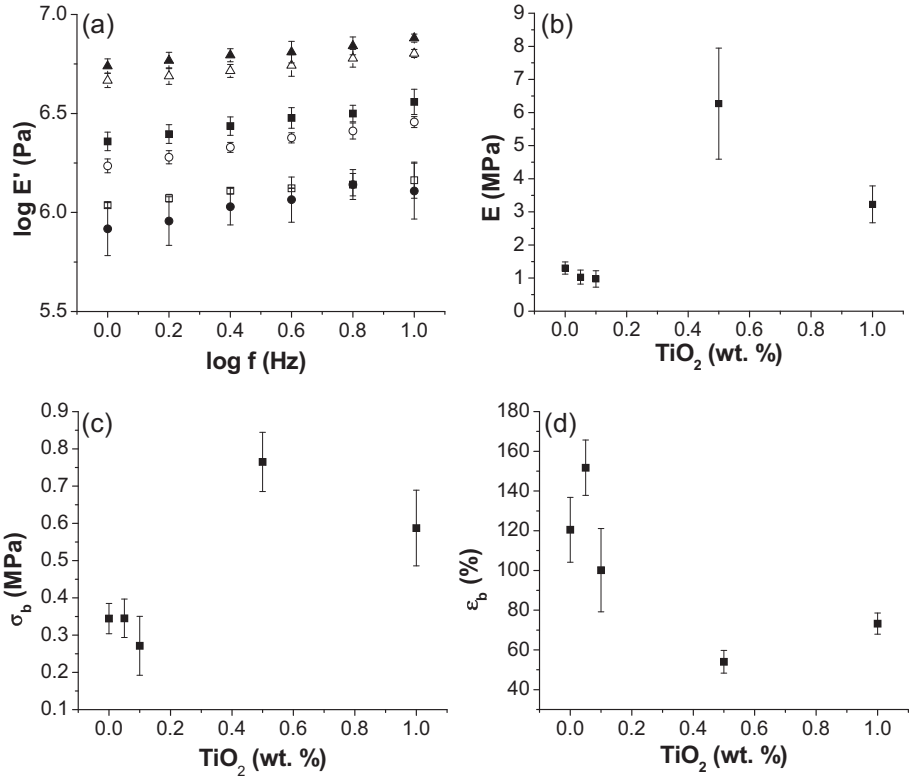

Fig. 1. Mechanical and tensile parameters for films prepared from conventional emulsions (CE) with different concentrations of TiO_2: (a) log E′ vs log f (frequency) with 0 (■), 0.05 (□), 0.10 (●), 0.30 (○), 0.50 (▲), and 1.0 wt % (Δ) TiO_2; (b) Young modulus, E; (c) the ultimate strength, σ_b; (d) elongation at break, ε_b.

preparing films with concentrations that varied from 0 to 3 wt%. Without glycerol, it was not possible to remove the film from the dish. With addition of 3 wt% the film lacks of elasticity. 2 wt% glycerol was the concentration that led to better mechanical and tensile properties (data not shown) and therefore this was the selected concentration for this study.

3.2. Mechanical and tensile properties of films

Table 1 summarizes the values of E′ and E″ obtained when the curve log E′ or log E″ vs. log f (frequency) intercepted y-axis for all films prepared in this study. To check the effect of lipid phase on mechanical properties, films prepared from solutions were also included in Table 1. No significant differences in E′ and E″ were obtained for solutions and conventional emulsions, indicating that the presence of SFO did not modify mechanical properties. This result is relevant for films intended to contain an active molecule in the lipid phase. Films with oil may be expected to perform as films from solutions. Similar results were published by Pereda et al. (2010) for caseinate films modified with tung oil. Films prepared from NE had similar mechanical properties than films from CE. When films came from gels prepared starting from CE or NE, they were very fragile and their mechanical properties could not be measured. Addition of TiO_2 improved rheological properties in all films and therefore E′ and E″ moduli were significantly higher than for films without charge (Table 1). CG and NG had the greatest E′ modulus of all, indicating that for some applications gels with charge could be the best option.

Table 2 summarizes tensile parameters for all films. No significant differences in E values were found for films prepared from S, CE, or NE ($p < 0.05$). Films prepared from CG and NG were too fragile to be measured by this technique. Parameters σ_b and ε_b were significantly higher for films obtained from S than CE and NE. Addition of TiO_2

Table 1
Initial values of storage (E′) and loss (E″) moduli for all films.

Film[1]	E′ (MPa)[3]	E″ (MPa)[3]
S	2.3 ± 0.1[a]	1.0 ± 0.1[a]
S T0.5	5.9 ± 0.3[b]	1.8 ± 0.1[b]
CE	2.3 ± 0.2[a]	0.9 ± 0.1[a]
CE T0.5	5.4 ± 0.2[b]	1.9 ± 0.1[b]
NE	2.7 ± 0.2[a]	0.8 ± 0.1[c]
NE T0.5	3.5 ± 0.1[c]	1.0 ± 0.1[a]
CG[2]	–	–
CG T0.5	12.6 ± 0.1[d]	2.9 ± 0.2[d]
NG[2]	–	–
NG T0.5	12.9 ± 0.1[d]	2.9 ± 0.2[d]

[1] Abbreviations: S film from sodium caseinate solution, CE film from conventional emulsion, NE film from nanoemulsion, CG film from conventional gel, NG film from nanogel, T TiO_2.

[2] CG and NG without TiO_2 were not measured because they broke when cutting for experiment.

[3] Data are expressed as mean values and standard deviations of three replicates. For E′ and E″, values with the same superscripts are not significantly different ($\alpha = 0.05$).

Table 2
Young modulus (E), the ultimate strength (σ_b), and elongation at break (ε_b) for all films.

Film[1]	E (MPa)[3]	σ_b (MPa)[3]	ε_b (%)[3]
S T0	1.0 ± 0.2[a]	0.54 ± 0.09[a]	206 ± 11[a]
S T0.5	1.5 ± 0.3[a]	0.70 ± 0.04[b]	173 ± 12[b]
CE T0	1.3 ± 0.2[a]	0.34 ± 0.04[c]	120 ± 16[c]
CE T0.5	6.3 ± 1.6[b]	0.77 ± 0.08[b]	54 ± 6[d]
NE T0	1.0 ± 0.2[a]	0.34 ± 0.05[c]	148 ± 15[c]
NE T0.5	2.4 ± 0.1[c]	0.48 ± 0.03[a]	56 ± 16[d]
CG[2] T0	–	–	–
CG T0.5	33.1 ± 3.5[d]	1.08 ± 0.03[d]	16 ± 3[e]
NG[2] T0	–	–	–
NG T0.5	41.8 ± 4.2[f]	0.85 ± 0.14[d]	10 ± 3[e]

[1] Abbreviations as in Table 1.

[2] CG and NG without TiO_2 were not measured because they broke when cutting for experiment.

[3] Data are expressed as mean values and standard deviations of eight replicates. For E, σ_b, and ε_b, values with the same superscripts are not significantly different ($\alpha = 0.05$).

Table 3
Water vapor permeability (WVP) and film thickness (e) for all films.

Film[1]	e (mm)	WVP[2] (g/Pa h m) × 10^7
S T0	0.18 ± 0.02[a]	2.35 ± 0.35[a]
S T0.5	0.17 ± 0.03[a]	3.33 ± 0.25[b]
CE T0	0.17 ± 0.04[a]	4.10 ± 0.32[c]
CE T0.5	0.18 ± 0.02[a]	4.51 ± 0.18[c]
NE T0	0.18 ± 0.04[a]	3.53 ± 0.08[b]
NE T0.5	0.16 ± 0.04[a]	4.33 ± 0.28[c]
CG T0	–	–
CG T0.5	0.19 ± 0.04[a]	4.23 ± 0.07[c]
NG T0	–	–
NG T0.5	0.19 ± 0.03[a]	3.84 ± 0.17[b]

[1] Abbreviations as in Table 1.
[2] Data are expressed as mean values and standard deviations of three replicates. For WVP values with the same superscripts are not significantly different (α = 0.05).

significantly increased parameter E for films from CE and NE. For films from S no significant differences were found. The systems formulated with a lipid phase became more elastic for addition of a charge. In the case of films CGT0.5 or NGT0.5 the charge modified tensile properties dramatically compared to the CG and NG films. Films became difficult to break as may be noticed from parameter E and σ_b values. In addition, ε_b significantly diminished for addition of 0.5 wt% TiO_2, indicating that less deformation occurred before breaking. The notable effect of TiO_2 on CG and NG clearly indicate a different interaction between TiO_2 nanoparticles and proteins. Although at present the reasons are not well known, it is remarkable that due to GDL acidification TiO_2 surface charge may shift to positive values improving protein-surface interaction (TiO_2 isoelectric point is close to pH = 6). Besides, as it will be discussed later, gelation led to a more homogeneous distribution of nanoparticles in the matrix. Both effects enhanced protein-TiO_2 interactions.

3.3. Water vapor permeability (WVP)

The WVP reflects the easiness of water vapor to pass through the film. Table 3 summarizes WVP and film thickness (e) for all films prepared. Films prepared from S displayed lower WVP than those from CE or NE. A similar effect was reported for films obtained from caseinate microemulsions (Pereda et al., 2010). This result may be a consequence of the presence of oil droplets in the films, which introduce defects that increase water permeability. Interestingly, this effect is lower in the case of the more homogeneous NE, supporting the previous hypothesis. Incorporation of TiO_2 nanoparticles increased a little more WVP with respect to the films without TiO_2, which can be also consequence of the formation of defects that may help the permeation of water vapor though small porous or holes. In previous work realized with WPI-caseinate-TiO_2 films, a reduction of WVP was observed with concentrations of TiO_2 lower than those used in this work (Lei et al., 2014). In the same work, an increment of WVP was observed as TiO_2% increased, which is in agreement with our findings. Lei et al. (2014) results indicated that the effects on TiO_2 were dependent on concentration.

3.4. Thermogravimetric properties

Fig. 2 shows TGA weight loss curves for all films. Films prepared from S, CE, and NE are reported in part (a) and their gels in part (b). The same formulations as for (a) and (b) with addition of 0.5 TiO_2 are shown in part (c) and (d), respectively. Percentage of loss at different temperature and of remaining mass (mass of sample at the end of thermal treatment) was summarized in Table 4. Films from S lost free water in a range of temperatures around 25 to 110 °C (a). It was reported that solution films formulated with 5% WPI and 2% NaCas lost free water adsorbed in the film between 20 and 160 °C (Lei et al., 2014). Associated water and glycerol were lost in the 110–220 °C and 250–350 °C range, respectively. Films from SG displayed a similar thermogravimetric profile, but the losses of mass were more stepped than in the S case (b). These differences may be related with the different microstructure of the films. The incorporation of TiO_2 to these films did not notably modify the decomposition profile, but appreciably reduced the amount of volatiles lost in the 250–350 °C range in the SG case (compare Fig. 2a and b with c and d respectively).

The decomposition patterns of the films obtained from CE or NE is different from the corresponding patterns of S. The mass lost in the 25–100 °C range is smaller, indicating that the amount of free water in these films is lower than in the S and SG films or that it was retained at higher temperatures (Table 4). Associated water and glycerol were lost at higher temperatures: 125–270 °C for CE and NE, and 140–280 °C for CG and NG. Oil decomposition started at approximately 330 °C and the remaining volatiles were lost in the 350–500 °C range (Table 4). TiO_2 incorporation did not produce important changes in the decomposition profiles of films from CET0.5, NET0.5 or CGT0.5. In the case of NGT0.5 the presence of TiO_2 notably reduced the loss of volatiles in the 250–350 °C range (as in the case of SGT0.5). This effect may be associated with a stronger interaction between water and TiO_2 in these cases.

3.5. Laser scanning confocal microscopy images

Fig. 3 reports confocal images of films formulated without TiO_2. The red color in images is the lipid phase. Films prepared from CE displayed flocs from the agglomeration of oil droplets, indicating that the oil is not homogeneously distributed in the material (a). During the casting process, droplets had time to interact and the final structure was not homogeneous. Films formed from CG structure were more homogeneous. Droplets appeared well distributed and less aggregated (b). Films from NE showed very small droplets (c). Due to their size, droplets in NE did not suffer gravitational destabilization and structure did not show droplets aggregation. Films from NG were very homogeneous (d). The higher homogeneity in oil droplets distribution observed in films from CG or NG with respect to those from CE or NE can be explained as a result of pH diminution due to GDL addition; droplets had low mobility after a few minutes of preparation and could not agglomerate. Fig. 4 shows representative images of all films containing 0.5 wt% TiO_2. Films from CET0.5 showed more homogeneous distribution of droplets than the corresponding films without TiO_2. However, aggregates were still noticeable (a). For films from CGT0.5, NET0.5, and NGT0.5, the addition of TiO_2 led to a more homogeneous distribution of droplets (b, c, and d) than in the corresponding samples without TiO_2. This result was in agreement with values of E′ (Table 1) and E, σ_b, and ε_b (Table 2). A more homogeneous droplets distribution corresponded to better mechanical and tensile properties.

3.6. Structure by SEM

Fig. 5 reports SEM images of films formulated without charge. Images correspond to surface exposed to air when drying. Part (a) shows morphology of the film obtained from solution (S). The CE film was not analyzed since oil droplets were released from the matrix and the image was blurry. Parts (b), (c), and (d) show films from NE, CG, and NG, respectively. The film from solution (S) contained protein agglomerates of different sizes (a). These agglomerates were smaller for the film from NE (b). The fact that CE released oil during measurements and NE did not, may be associated with the stability of nanoemulsions when compared to emulsions. The former are much more stable against flocculation and coalescence than the latter (Ebert, Koo, Weiss, & McClements, 2017). Distribution of oil in the films in the form of nanodroplets may explain this behavior. To prove this hypothesis, characterization of films by SAXS was performed, as it will be discussed later. These results show that using NE may be an advantage if more

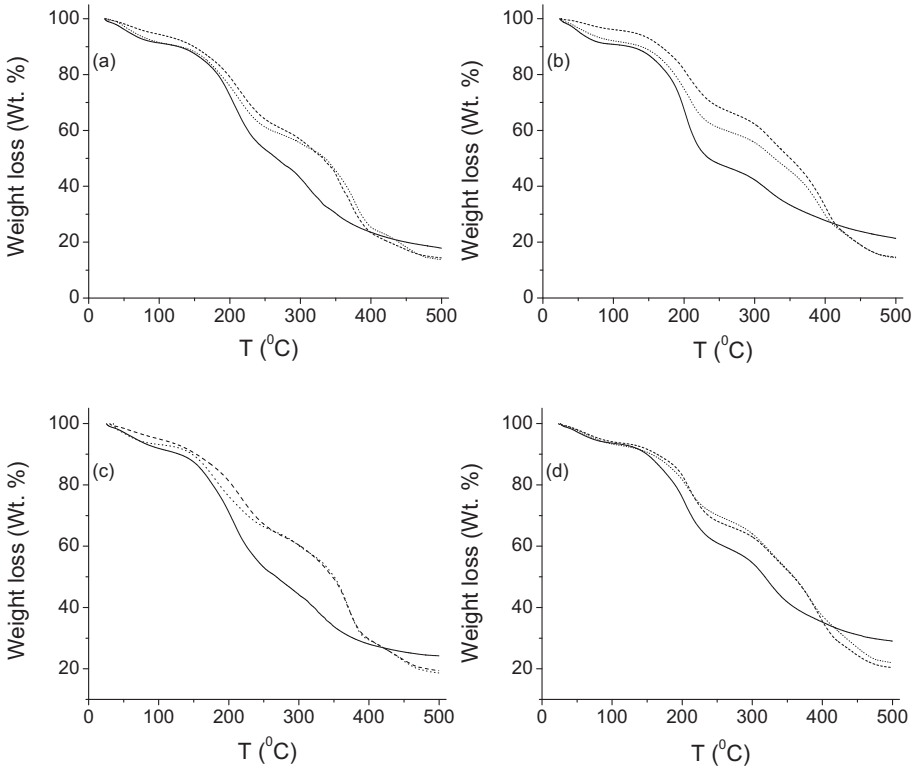

Fig. 2. Thermo-gravimetric analysis (TGA) of all films prepared from: (a) —— S, ———— CE, ■■■■■■■ NE; (b) —— SG, ———— CG, ■■■■■■■ NG; (c) —— ST0.5; ———— CET0.5; ■■■■■■■ NET0.5; d) —— SGT0.5; ———— CGT0.5; ■■■■■■■ NGT0.5.

Table 4
TGA weight loss at different temperatures and final weight for all films.[2]

Film[1]	100 °C (%)	250 °C (%)	290 °C (%)	500 °C (%)	Final mass (%)
S T0	8.69^{a}	38.09^{a}	7.77^{a}	27.61^{a}	17,84^{a}
S T0.5	8.08^{a}	38.84^{a}	7.05^{a}	21.80^{b}	24.23^{b}
CE T0	5.60^{b}	30.36^{b}	5.61^{b}	44.07^{c}	14.36^{c}
CE T0.5	4.99^{b}	27.85^{b}	5.40^{b}	42.37^{c}	19.39^{a}
NE T0	8.48^{a}	30.31^{b}	4.43^{b}	43.02^{c}	13.76^{c}
NE T0.5	6.82^{b}	26.87^{b}	4.45^{b}	43.21^{c}	18.65^{a}
SG T0	9.20^{c}	42.82^{c}	4.18^{b}	22.46^{b}	21.34^{d}
SG T0.5	6.39^{b}	32.56^{d}	4.69^{b}	27.30^{a}	29.06^{e}
CG T0	3.89^{d}	27.84^{b}	4.49^{b}	49.16^{d}	14.62^{c}
CG T0.5	5.93^{b}	25.90^{e}	3.86^{b}	43.91^{c}	20.40^{d}
NG T0	7.93^{a}	31.22^{d}	3.83^{b}	42.62^{c}	14.40^{c}
NG T0.5	6.68^{b}	23.20^{e}	4.42^{b}	43.69^{c}	22.01^{d}

[1] Abbreviations as in Table 1.
[2] Data are expressed as mean values of two replicates. Values in the same column with the same superscripts are not significantly different (α = 0.05).

stable films are needed. Films from gels had a very different morphology than films without GDL. During gelation, protein micelles interact to each other to form a 3D network that includes oil droplets. Building blocks were greater for CG (c) than for NG (d) and therefore the 3D network was less homogeneous in (c) than in (d). Films in (c) showed great round protein structures that were not present in films in (d).

Fig. 6 shows SEM images for the films analogous to Fig. 5 but with addition of 0.5 wt% TiO_2. The presence of TiO_2 strongly modified protein agglomeration. The round protein structures were smaller than in the corresponding films without charge. Although TiO_2 incorporation could not prevent oil release in sample CE T0.5, films showed a more homogeneous distribution of aggregates which is in agreement with the improvement in mechanical and tensile properties.

Fig. 7 reports cryogenic fracture surfaces of films prepared from CG T0.5 and NG T0.5. As may be noticed, no sedimentation of TiO_2 particles occurred. Bottom edge images (a, c) did not show accumulation of TiO_2. CG had more pores than NG. In addition, pores had a greater diameter and a less homogeneous distribution. Mechanical and tensile properties of films with TiO_2 were significantly different for gels compared to emulsions. In agreement with these differences, structures were strongly modified by the charge in terms of pore size and distribution. CG showed a less homogeneous structure than NG. As explained in Section 3.3, structures with defects made a worse barrier to WVP. In agreement with this tendency, WVP was higher for CG than for NG.

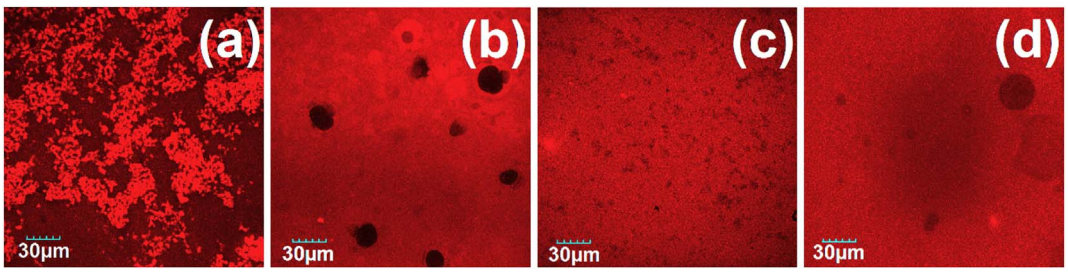

Fig. 3. Confocal images of films formulated without TiO_2, prepared from: (a) conventional emulsion (CE); (b) gel from conventional emulsion (CG); (c) nanoemulsions (NE); (d) gel from nanoemulsions (NG). Nile red was used as dye. (For interpretation of the references to color in this figure, the reader is referred to the web version of this article.)

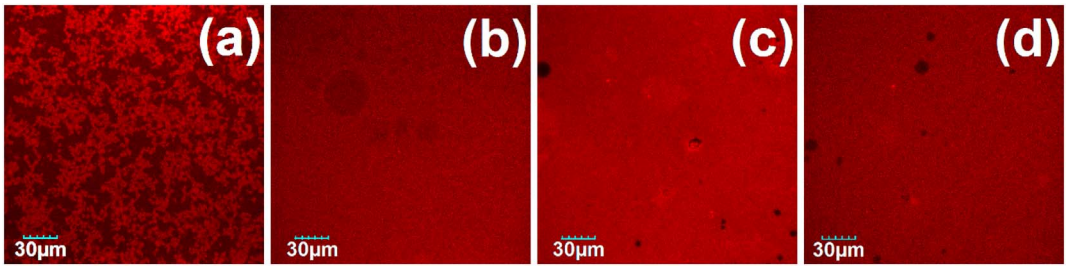

Fig. 4. Confocal images for films containing 0.5 wt% TiO_2 prepared from: (a) conventional emulsions (CE); (b) gel from conventional emulsions (CG); (c) nanoemulsions (NE); (d) gel from nanoemulsions (NG). Nile red was used as dye.

3.7. X-rays: SAXS and WAXS

Small angle X-ray scattering microscopies, the relevant transmission microscopies and normalized scattered intensity maps are shown in Fig. 8 (left, central, and right columns, respectively). The edge of the sample is represented by the border line between the blue and colored regions in the scattering maps (and vice versa in the transmission maps). The basically uniform color in the scanning SAXS 2D maps demonstrates the high degree of sample homogeneity on a ~100 μm scale, and hence the even distribution of the TiO_2 nanoparticles, in TiO_2 loaded samples, with no significant segregation in the investigated area. This can also be appreciated by plotting several scattering profiles from consecutive points on the sample, either in the small (as e.g. in Fig. S1) or in the wide (Fig. S2) angle range. Even by crossing regions of the SAXS microscopies with color changing from red to yellow, no significant differences resulted in the SAXS nor in the WAXS profiles for most of the films. It is worth noting that small angle X-ray scattering curves did not show features (fringes or correlation peaks) typical of objects with well-defined morphology (see e.g. Fig. S1), although it appears that samples can be grouped based on tiny differences in the slope of the SAXS curves (Fig. S3). As a result, some nanoscale similarity can be recognized between the films from NE and NG, as well as between samples charged with TiO_2 nanoparticles. The data corresponding to the films from CE, stay far from the others, confirming the different length scales in its structure, as expected. Moreover, besides oil droplets and TiO_2 nanoparticles, the whole matrix is contributing to the scattering from each sample, which can be hardly subtracted from the SAXS pattern as the "buffer" in typical SAXS experiments on solutions, in order to isolate the scattering signal from nano-objects. Indeed, even the derived D_{max} and R_g values (Table 5) were found not to be directly representative of the size of the particles in the films, being basically unchanged even independently of the TiO_2 load, although CE films are overall characterized by larger R_g and D_{max} values compared to NE and NG films.

The values of D_{max} and R_g in polydisperse systems are related to the largest and average size of the objects, respectively, whereby they are not to be considered as structural details of the individual objects. Indeed, the obtained values reported in Table 5 only provide a qualitative indication of tiny differences in sample nanostructure. On the other hand, a different approach based on the evaluation of the q-dependent scattering intensity (q being the scattering vector modulus) was adopted, and quantitative information related to sample nanostructure could be derived, as explained in the following. A statistical average was obtained by integrating the SAXS intensity in a specific q-

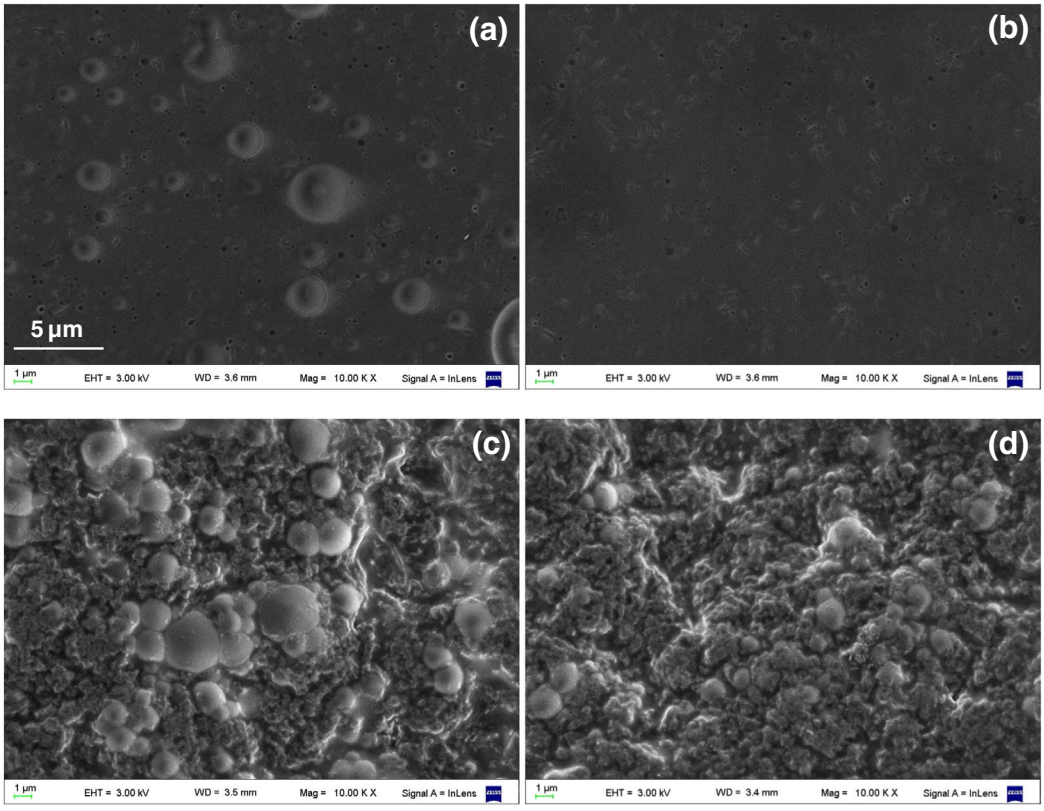

Fig. 5. SEM images for films without TiO_2 prepared from: (a) solution (S); (b) nanoemulsions (NE); (c) conventional gel (CG); and (d) nanogel (NG).

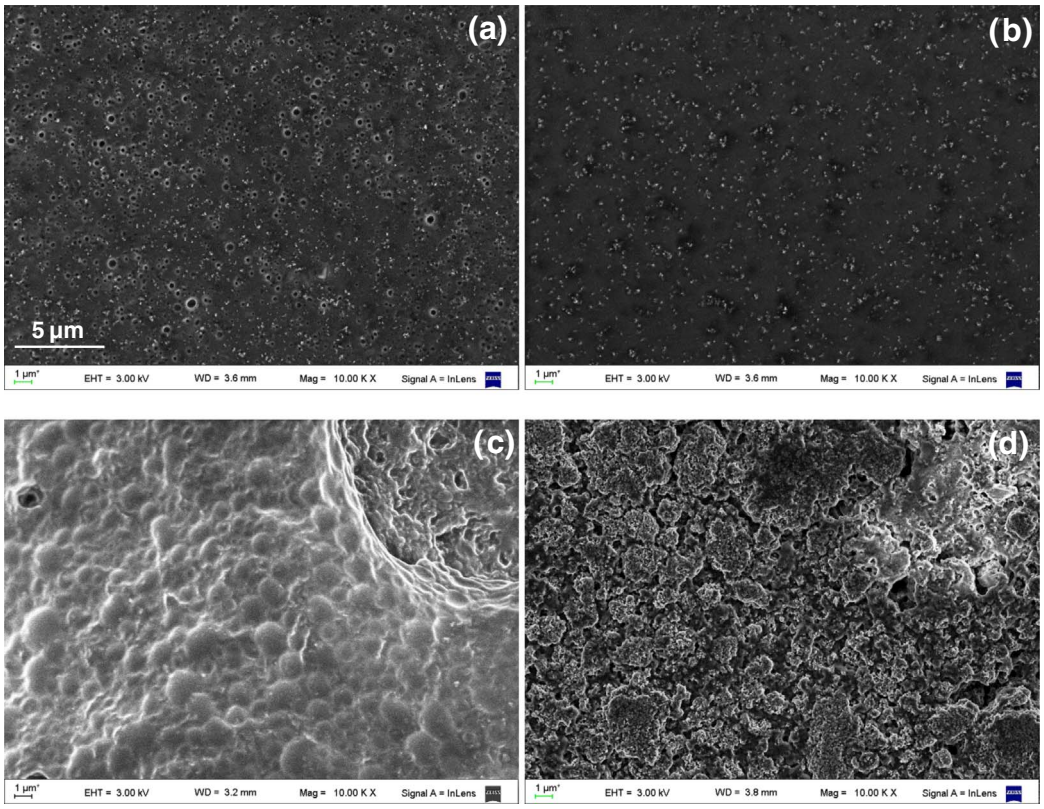

Fig. 6. SEM images for films with 0.5 wt% TiO_2 prepared from: (a) solution (S); (b) nanoemulsions (NE); (c) conventional gel (CG); and (d) nanogel (NG).

range (0.01–0.1 $Å^{-1}$), where most of the scattering intensity is found and is well above the background level (see e.g. Fig. S1), and then averaging over all patterns (approximately 500) collected from a given area (~4 × 4 mm^2) of the sample (see drawing in Fig. S4). Such an approach was already shown to provide length scale dependent quantitative statistical information, over large sample areas, about

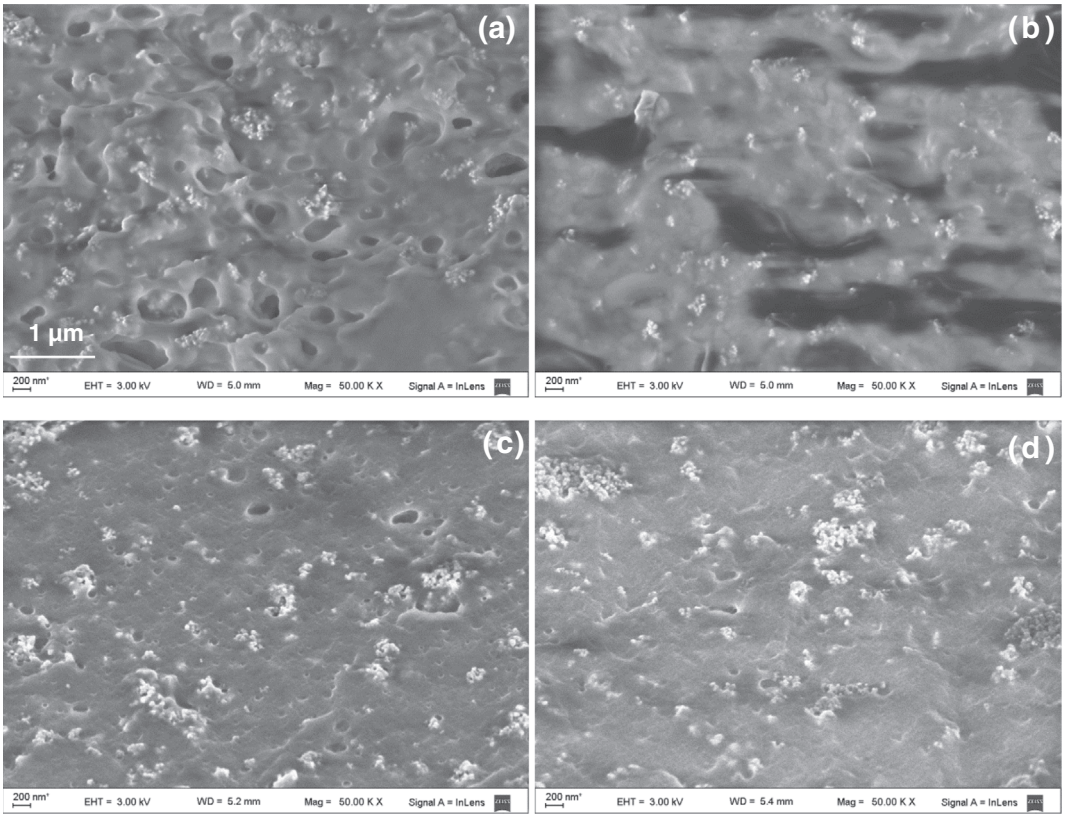

Fig. 7. Cross sectional surfaces of films. (a, b) Prepared from conventional gel (CG); (c, d) prepared from nanogel (NG). (a, c) Bottom edge. (b, d) Top edge. Magnification was 50.000 ×.

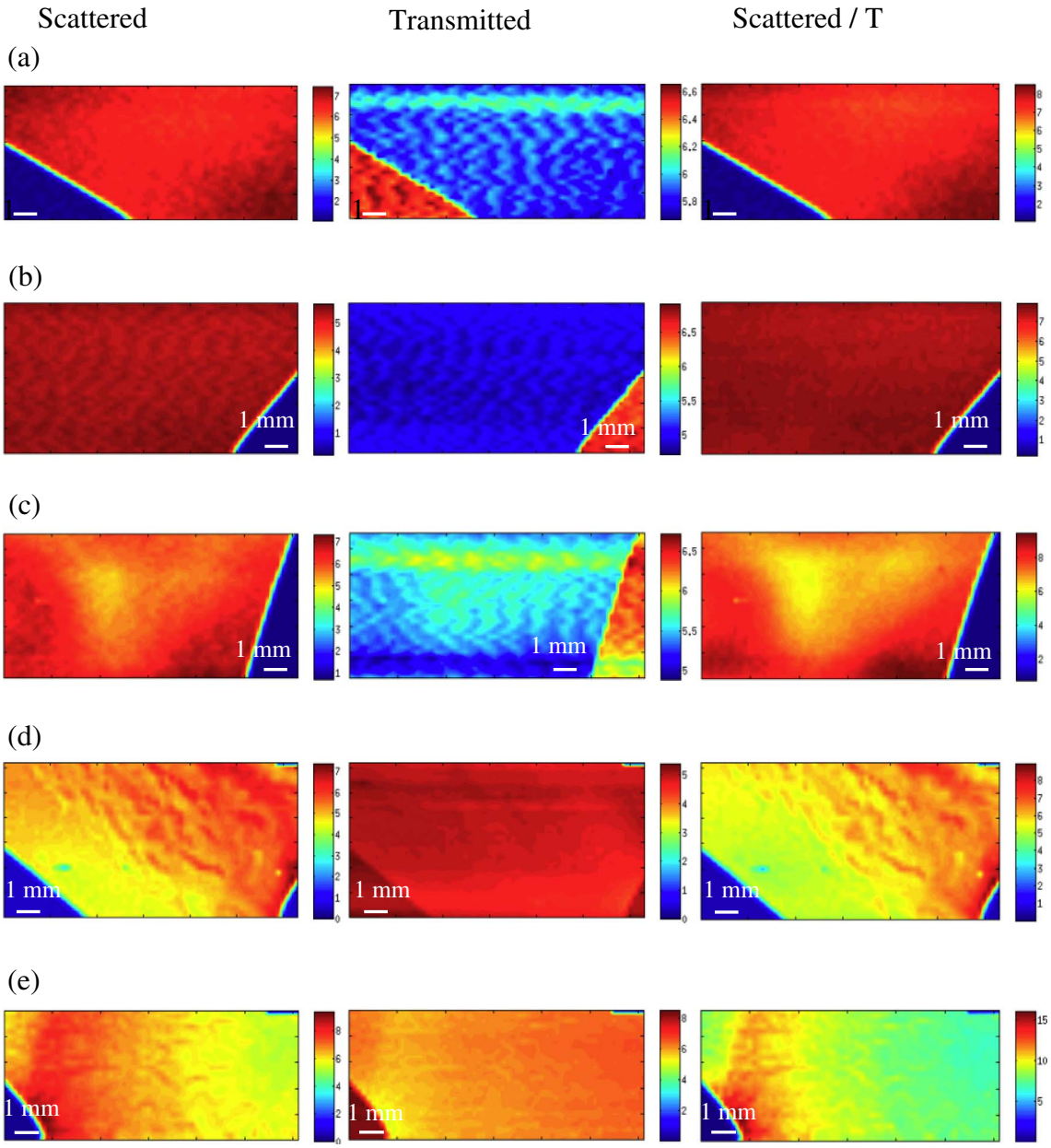

Fig. 8. Scattered (left column) transmitted (central column), and normalized scattered intensity to the transmission coefficient (right column) as derived from the transmission intensity map for NE films without (a) and with (b) TiO_2; for NG films without TiO_2 (c); for CE without (d) and with (e) TiO_2. All numbers in the color bars are multiplied by $= 10^{-4}$. (For interpretation of the references to color in this figure legend, the reader is referred to the web version of this article.)

Table 5
Value of D_{max} and R_g for selected films showing qualitative information of nanostructure.

Sample	NE	NET0.5	NG	CE	CET0.5
D_{max} (nm)	42.3	46.0	41.2	64.5	54.3
R_g (nm)	14.2	16.5	14.6	27.5	28.1
	12.2	15.2	13.1	21.3	17.3
SAXS intensity	941	2985	541	263	3322

nanoparticle distributions over 2D slices of inhomogeneous samples (Altamura et al., 2016), and has been confirmed here as a valuable tool in the study of samples with nanoscale inhomogeneity/polydispersity. The overall SAXS intensity, normalized to collection time, beam intensity and transmission factor, was indeed found to be clearly sample-dependent, indicating the presence of nano-objects (mainly below or slightly above 100 nm in size, based on the accessible q-range) with significantly different scattering power and/or concentration (film thickness is in all cases 0.18 ± 0.01 mm). The resulting normalized intensity values, reported in Table 5 readily show that a much larger scattering intensity is detected in films charged with TiO_2 compared to the analogous without charge, in particular by a factor 5.5 for the NE films and 12.6 for the CE films. Therefore the presence of the TiO_2 charge clearly shines, and is confirmed by the characteristic diffraction peaks in the WAXS patterns (Fig. S2). Its presence is also reflected in the measured transmission coefficient, which was on average lower by about 10% in the samples charged with TiO_2 (0.8 compared to 0.9 in samples without charge).

Table 5 also shows differences among emulsions without TiO_2 charge. In particular, the highest SAXS intensity was collected from NE films, being a factor 3.6 larger than the intensity from the CE films (lowest value). The SAXS intensity from the NG films is found in between.

Such results indicate that the nanostructure character of the nanoemulsions is retained in the corresponding films, with possibly a larger concentration of nanodroplets in the NE films compared to the NG films. Finally, the scanning approach with intensity evaluation allows to better highlight sample inhomogeneities. The largest color difference on extended areas in SAXS microscopies was found for the CE films, with or without TiO_2 charge, between the red and yellow regions (see Fig. 8), which corresponds to a 20–30% intensity variation on average (which can be also recognized in the WAXS profiles, Fig. S2). Being such variations independent of the presence of TiO_2, they appear as due to intrinsic inhomogeneities of the CE films. Some local variations of the same order can be recognized in small regions of the NE films, which although show on average higher homogeneity, in particular when they are charged with TiO_2.

4. Conclusions

Natural-biopolymer films based on NaCas/glycerol/SFO for food applications were obtained by solvent-casting evaporation method. Films prepared from CE or NE had similar mechanical behavior than films from S, indicating that the presence of a well distributed lipid phase did not appreciably modified the mechanical properties of caseinate films. Films prepared from CG and NG were too fragile for practical applications, showing that preparation conditions are decisive for films characteristics. However, the mechanical and tensile properties of films were improved by addition of TiO_2 as charge because structure was improved in terms of size and distribution of oil droplets and protein aggregates. SAXS/WAXS analyses were effective in confirming a homogeneous distribution of TiO_2 and a higher intrinsic homogeneity of NE films compared to CE films, independently of the TiO_2 charge addition. Higher homogeneity in the structure led to improved physical properties such as water vapor permeability and stability with respect to oil release. These set of new sodium caseinate based films, have interesting potential applications as functional materials because bioactive compounds may be dissolved in the oil phase. For example the NE films displayed similar mechanical and WVP properties to S films, containing very stable and well distributed oil nanodroplets that may contain dissolved antioxidants or vitamins.

Author contributions

J. M. M. de O. A., R. J. C. and M. L. H. prepared all samples, performed mechanical, thermal characterization, WVP and SEM studies. D. A. and C. G. performed X-ray characterization. D. S. and F. S. contributed to X-ray data analysis. R. J. C., M. L. H., D. A. and C. G. contributed to manuscript preparation, which was discussed with all the authors. All authors have given approval to the final version of the manuscript.

Funding sources

This work was supported by the International CONICET-Argentina/CNR-Italy Bilateral Project entitled "TiO_2 caseine polymeric composite films for food preservation", the National Agency for the Promotion of Science and Technology (ANPCyT) through Project PICT 2013-0897, and by the University of Buenos Aires through Project UBA-20020130100136BA.

Acknowledgment

Roberto Lassandro is acknowledged for its technical support in the XMI-Lab of CNR-IC.

Appendix A. Supplementary data

SAXS and WAXS profiles, composite SAXS maps. Supplementary data associated with this article can be found in the online version, at https://doi.org/10.1016/j.foodres.2017.11.011.

References

Acevedo-Fani, A., Salvia-Trujillo, L., Rojas-Grau, M. A., & Martín-Belloso, O. (2015). Edible films from essential-oil-loaded nanoemulsions: Physicochemical characterization and antimicrobial properties. *Food Hydrocolloids, 47*, 168–177.

Altamura, D., Lassandro, R., Vittoria, F. A., De Caro, L., Siliqi, D., Ladisa, M., & Giannini, C. (2012). X-ray MicroImaging laboratory (XMI-LAB). *Journal of Applied Crystallography, 45*, 869–873.

Altamura, D., Pastore, S. G., Raucci, M. G., Siliqi, D., De Pascalis, F., Nacucchi, M., ... Giannini, C. (2016). Scanning small- and wide-angle X-ray scattering microscopy selectively probes HA content in gelatin/hydroxyapatite scaffolds for osteochondral defect repair. *ACS Applied Materials and Interfaces, 8*, 8728–8736.

Arrieta, M. P., Peltzer, M. A., Garrigós, M. C., & Jiménez, A. (2013). Structure and mechanical properties of sodium and calcium caseinate edible active films with carvacrol. *Journal of Food Engineering, 114*, 486–494.

Arrieta, M. P., Peltzer, M. A., López, J., Garrigós, M. C., Valente, A. J. M., & Jiménez, A. (2014). Functional properties of sodium and calcium caseinate antimicrobial active films containing carvacrol. *Journal of Food Engineering, 121*, 94–101.

Atarés, L., Bonilla, J., & Chiralt, A. (2010). Characterization of sodium caseinate-based edible films incorporated with cinnamon or ginger essential oils. *Journal of Food Engineering, 100*, 678–687.

Bonilla, J., & Sobral, P. J. A. (2017). Antioxidant and physicochemical properties of blended films based on gelatin-sodium caseinate activated with natural extracts. *Journal of Applied Polymer Science, 134*. http://dx.doi.org/10.1002/app.44467.

Cinelli, P., Schmid, M., Bugnicourt, E., Wildner, J., Bazzichi, A., Anguillesi, I., & Lazzeri, A. (2014). Whey protein layer applied on biodegradable packaging film to improve barrier properties while maintaining biodegradability. *Polymer Degradation and Stability, 108*, 151–157.

Colak, B. Y., Gouanve, F., Degraeve, P., Espuche, E., & Prochazka, F. (2015). Study of the influences of film processing conditions and glycerol amount on the water sorption and gas barrier properties of novel sodium caseinate films. *Journal of Membrane Science, 478*, 1–11.

Ebert, S., Koo, C. K. W., Weiss, J., & McClements, D. J. (2017). Continuous production of core-shell protein nanoparticles by antisolvent precipitation using dual-channel microfluidization: Caseinate-coated zein nanoparticles. *Food Research International, 92*, 48–55.

Fabra, M. J., Talens, P., Gavara, R., & Chiralt, A. (2012). Barrier properties of sodium caseinate films as affected by lipid composition and moisture content. *Journal of Food Engineering, 109*, 372–379.

Famá, L., Rojo, P. G., Bernal, C., & Goyanes, S. (2012). Biodegradable starch based nanocomposites with low wáter vapor permeability and high storage modulus. *Carbohydrate Polymers, 87*, 1989–1993.

Franke, D., Petoukhov, M. V., Konarev, P. V., Panjkovich, A., Tuukkanen, A., Mertens, H. D. T., ... Svergun, D. I. (2017). ATSAS 2.8: A comprehensive data analysis suite for small-angle scattering from macromolecular solutions. *Journal of Applied Crystallography, 50*, 1212–1225.

Frohberg, P., Pietzsch, M., & Ulrich, J. (2010). Effect of crystalline substances in biodegradable films. *Chemical Engineering Research and Design, 88*, 1148–1152.

Helal, A., Tagliazucchi, D., Conte, A., & Desobry, S. (2012). Antioxidant properties of polyphenols incorporated in casein/sodium caseinate films. *International Dairy Journal, 25*, 10–15.

Hwang, S. Y., Yoo, E. S., & Im, S. S. (2011). Effects of TS-1 zeolite structures on physical properties and enzymatic degradation of poly (butylene succinate) (PBS)/TS-1 zeolite hybrid composites. *Polymer, 52*, 965–975.

Jiménez, A., Fabra, M. F., Talens, P., & Chiralt, A. (2013). Physical properties and antioxidant capacity of starch–sodium caseinate films containing lipids. *Journal of Food Engineering, 116*, 695–702.

Lee, S. J., & McClements, D. J. (2010). Fabrication of protein-stabilized nanoemulsions using a combined homogenization and amphiphilic solvent dissolution/evaporation approach. *Food Hydrocolloids, 24*, 560–569.

Lei, Q., Huang, Z., Pan, J., Bao, J., Xun, Q., Jiang, S., & Zhang, Y. (2014). Research on antimicrobial activity and packaging performance of degradable protein films. *Advanced Materials Research, 915-916*, 947–953.

Li, Y., Jiang, Y., Liu, F., Ren, F., Zhao, G., & Leng, X. (2011). Fabrication and characterization of TiO_2/whey protein isolate nanocomposite film. *Food Hydrocolloids, 25*, 1098–1104.

Matsakidou, A., Biliaderis, C. G., & Kiosseoglou, V. (2013). Preparation and characterization of composite sodium caseinate edible films incorporating naturally emulsified oil bodies. *Food Hydrocolloids, 30*, 232–240.

Moditsi, M., Lazaridou, A., Moschakis, T., & Biliaderis, C. G. (2014). Modifying the physical properties of dairy protein films for controlled release of antifungal agents. *Food Hydrocolloids, 39*, 195–203.

Morales, L., Franco, L., Casas, M. T., & Puiggali, J. (2010). Crystallization behavior of clay nanocomposites prepared from a degradable alternating copolyester constituted by glycolic acid and 6-hydroxyhexanoic acid. *Journal of Polymer Science: Polymer Physics, 48*, 33–46.

Navarro, R., Arancibia, C., Herrera, M. L., & Matiacevich, S. (2016). Effect of type of encapsulating agent on physical properties of edible films based on alginate and thyme oil. *Food and Bioproducts Processing, 97*, 63–75.

Pereda, M., Aranguren, M. I., & Marcovich, N. E. (2010). Caseinate films modified with tung oil. *Food Hydrocolloids, 24*, 800–808.

Perez-Gago, M. B., & Krochta, J. M. (2001). Lipid particle size effect on water vapor permeability and mechanical properties of whey protein/beeswax emulsion films. *Journal of Agricultural and Food Chemistry, 49*, 996–1002.

Reznavi, E., Schleining, G., Sümen, G., & Taherian, A. R. (2013). Assessment of physical and mechanical properties of sodium caseinate and stearic acid based film-forming emulsions and edible films. *Journal of Food Engineering, 116*, 598–605.

Siliqi, D., De Caro, L., Ladisa, M., Scattarella, F., Mazzone, A., Altamura, D., ... Giannini, C. (2016). SUNBIM: A package for X-ray imaging of nano- and biomaterials using SAXS; WAXS; GISAXS and GIWAXS techniques. *Journal of Applied Crystallography, 49*, 1107–1114.

Svergun, D. I. (1992). Determination of the regularization parameter in indirect-transform methods using perceptual criteria. *Journal of Applied Crystallography, 25*, 495–503.

Tsai, C. C., Wu, R. J., Cheng, H. Y., Li, S. C., Siao, Y. Y., Kong, D. C., & Jang, G. W. (2010). Crystallinity and dimensional stability of biaxial oriented poly(lactic acid) films. *Polymer Degradation and Stability, 95*, 1292–1298.

Valencia-Chamorro, S. A., Palou, L., del Río, M. A., & Pérez-Gago, M. B. (2011). Antimicrobial edible films and coatings for fresh and minimally processed fruits and vegetables: A review. *Critical Reviews in Food Science and Nutrition, 51*, 872–900.

Wang, K., Jiao, T., Wang, Y., Li, M., Li, Q., & Shen, C. (2013). The microstructures of extrusion cast biodegradable poly(butylene succinate) films investigated by X-ray diffraction. *Materials Letters, 92*, 334–337.

Wihodo, M., & Moraru, C. I. (2013). Physical and chemical methods used to enhance the structure and mechanical properties of protein films: A review. *Journal of Food Engineering, 114*, 292–302.

Zhou, J. J., Wang, S. Y., & Gunasekaran, S. (2009). Preparation and characterization of whey protein film incorporated with TiO_2 nanoparticles. *Journal of Food Science, 74*, N50–N56.

Zinoviadou, K. G., Koutsoumanis, K. P., & Biliaderis, C. G. (2009). Physico-chemical properties of whey protein isolate films containing oregano oil and their antimicrobial action against spoilage flora of fresh beef. *Meat Science, 82*, 338–345.